Enhancement of thermographic images as tool for structural analysis in earthquake engineering

F. Cluni[a,*], D. Costarelli[b], A. M. Minotti[c], G. Vinti[c]

[a] *Department of Civil and Environmental Engineering, University of Perugia, Italy*
[b] *Department of Mathematics and Physics, Section of Mathematics, University of Roma Tre, Italy*
[c] *Department of Mathematics and Computer Sciences, University of Perugia, Italy*

Abstract

In this paper, we present an application of a reconstruction method to thermographic images employed to analyze the response of a masonry structure under seismic actions.

At first the theory of linear multivariate sampling Kantorovich operators are presented. By means of the above operators, we are able to reconstruct images taken from thermographic survey of masonry walls, and to enhance their quality. Digital image processing of reconstructed images allows us to identify the mutual arrangement of the blocks (made of stones and/or bricks) and mortar joints inside the wall portion analyzed, and therefore the texture of the masonry. Subsequently, the texture has been used to estimate the equivalent elastic properties of the masonry by means of homogenization techniques. Finally a real-world case-study is analyzed, taking into account the mechanical properties estimated from reconstructed thermographic images and evaluating the structural response in terms of modal analysis.

Keywords: Sampling Kantorovich operators, Digital image processing, Thermographic images, Homogenization, Structural analysis.

1. Introduction

In recent years, several researchers highlighted the advantages of using thermography in civil engineering applications [1, 2, 3]. Thermography is a remote sensing technique, performed by the image acquisition in the infrared, and therefore belongs to the family of non-destructive test for structures [4]. A survey of possible applications can be found in [5]. In particular, thermographic images can be used to make non-invasive investigations of structures, to analyze the story of the building wall, to make diagnosis and monitoring of buildings, and to make structural measurements.

The main use of thermography in civil engineering applications has been in the analysis of energetic performance of buildings, in particular to detect heat bridges and to assess the behavior at different seasons (see, for example, [6]); this is somehow similar to the heat transfer measurement in wind tunnel [7]. Subsequently, the possibility of using thermography as a non-destructive test has been acknowledged, with the further advantage of the possibility to analyze the building without

*Corresponding author
Email addresses: federico.cluni@unipg.it (F. Cluni), costarel@mat.uniroma3.it (D. Costarelli), annamaria.minotti@dmi.unipg.it (A. M. Minotti), gianluca.vinti@unipg.it (G. Vinti)

contact and rapidly, with consequent advantages in terms of operativeness and costs. For instance, thermography can be used to measure the moisture contents on surface and to detect imperfections on the substrate [8], to reveal small defects on concrete elements [9], to assess actual conditions and internal compositions of bridges [10]. Applications to evaluate the conditions of masonry and historical structures are also available [11, 12].

Unfortunately, the direct use of thermographic images can produce errors due to their low quality [13]. Therefore, several methods have been proposed in order to enhance the quality of thermographic images [14, 15, 16].

In the present paper, thermographic images are used both to assess effective dimensions of structural elements and for masonry texture, i.e., for the identification of the bricks and the mortar in masonries' images. The use of low quality images can induce errors when the image texture algorithm is used: in particular, an incorrect separation between the bricks and the mortar can occur. To enhance the quality of the thermographic images, reconstruction methods based on the theory of sampling Kantorovich operators are employed, and they have proved very useful for the applications here considered. The reconstruction methods are used to estimate the mechanical characteristics of the masonry walls of a case-study. It is worth noting that the interest of the present paper is not in the actual evaluation of the structural response of the case study to earthquake loads but rather in the applicability of the proposed procedure and the advantages that can be achieved in comparison with more traditional approaches. Furthermore, the proposed approach allows us to estimate the mechanical characteristics of the masonries using non-destructive methods.

The structure of the paper is the following: in Sec. 2 a brief introduction to thermography is given, with discussion of shortcomings when used for civil engineering applications; in Sec. 3 the application of the theory of sampling Kantorovich operators to reconstruct and to enhance the quality of thermographic images is presented: the reconstruction algorithm has been performed using MATLAB. In Sec. 4 the methods to estimate the mechanical characteristics of masonry wall using reconstructed thermographic images are described; in Sec. 5 an application to a case study is proposed; eventually, results are discussed in conclusions.

2. Thermography and its applications to civil engineering

Thermography is a technique which allows to appreciate and measure the heat flux associated with infrared radiation emitted from every body without direct contact, therefore it supplies a non-invasive technique for investigating buildings. The thermography is therefore a remote sensing technique, which exploit the fact that all the objects at a temperature above absolute zero emit radiation in the infrared range (wave length of 700 nm–1 mm, which corresponds to frequencies of 430 THz–300 GHz), which is located between the visible radiation (in particular the red component) and the microwave range.

The result of a thermographic survey is a bi-dimensional image, which is a thermic mapping of the heat flux of the body converted in temperature as will be detailed later. The measure of the surface temperature is indirect, since the thermographic cameras are only able to measure the input energy. Therefore, the quantity and quality of information which can be collected about the body examined strongly depends on the quality of the bi-dimensional image obtained from thermographic camera.

The radiation energy is measured by means of an infrared detector, which is able to absorb the incident energy and convert it in an electric signal. The main characteristic of the detector used in thermography is the reduced time elapsed from energy absorption to its conversion in electric

signal, in the order of μs. The main parameters of the detector are its image resolution and intensity resolution [17]. The image resolution is the ability to accurately detect and measure the surface temperature of the bodies even if they have small size. The intensity resolution is the ability to appreciate small temperature differences in the body.

As stated in the introduction, the thermographic images are largely used to make diagnosis and monitoring of buildings. They can also be used for structural survey, for example in the location and quantification of the resisting elements.

In the present paper, thermographic images will be used in the latter sense cited above, and moreover to investigate the actual texture of the masonry wall, i.e., the mutual arrangement of blocks and mortar joints. Anyway, the image resolution is often too low to achieve consistent results, and therefore reconstruction techniques described in the following section will be used.

3. Image reconstruction by multivariate sampling Kantorovich operators

In this section, we recall the theory of multivariate sampling Kantorovich operators and we describe their applications to image processing. In particular, we will apply these operators to thermographic images, for which we will study the texture to perform structural analysis.

The sampling Kantorovich operators have been introduced in [18] in a univariate setting and in [19] in a multivariate setting and they are related to the generalized sampling operators (see e.g. [20, 21, 22, 23, 24, 25, 26, 27, 28, 29, 30, 31, 32]).

More in detail, the sampling Kantorovich operators (1), below defined, represent an averaged version of the generalized sampling operators introduced by P.L. Butzer and his school at Aachen, and they in turn furnish a rigorous theory of an approximate version of the classical Whittaker-Kotelnikov-Shannon sampling theorem, very useful for the applications, see e.g. [20, 25, 33, 34, 35, 36]. In the Kantorovich case, instead of the evaluation of the signal f at the nodes $\underline{k}/w$, $\underline{k} \in \mathbb{Z}^n$, $w > 0$ (or $t_{\underline{k}}/w$ in the case of a non-uniform sampling scheme, where $(t_{\underline{k}})_{\underline{k}\in\mathbb{Z}^n}$ is a suitable sequence), we have an average of f on a small multi rectangle around $\underline{k}/w$. Practically, more information is usually known around a point than precisely at that point, and this procedure simultaneously reduces time-jitter errors. The algorithm deduced from the theory based on sampling Kantorovich operators, and discussed in Section 3.1, revealed to be very suitable for reconstruction processes, even in comparison with other approaches. Furthermore, the definition of the sampling Kantorovich operators is more suitable for the reconstruction of signals/images not necessarily continuous, and this fact plays an important role in image processing. This is an added value of these operators with respect to others, and in particular to the generalized sampling ones, since the latter depend on single function values $f(\underline{k}/w)$, and therefore not suitable in case of discontinuous functions.

Now, we recall the definition of the multivariate sampling Kantorovich operators. In what follows, we denote by $t_{\underline{k}} = (t_{k_1}, ..., t_{k_n})$ a vector where each $(t_{k_i})_{k_i\in\mathbb{Z}}$, $i = 1, ..., n$ is a sequence of real numbers with $-\infty < t_{k_i} < t_{k_{i+1}} < +\infty$, $\lim_{k_i\to\pm\infty} t_{k_i} = \pm\infty$, for every $i = 1, ..., n$, and such that there exists Δ, $\delta > 0$ for which $\delta \leq \Delta_{k_i} := t_{k_{i+1}} - t_{k_i} \leq \Delta$, for every $i = 1, ..., n$.

A function $\chi : \mathbb{R}^n \to \mathbb{R}$ will be called a kernel if it satisfies the following properties:

(χ1) $\chi \in L^1(\mathbb{R}^n)$ and is bounded in a neighborhood of $\underline{0} \in \mathbb{R}^n$;

(χ2) For every $\underline{u} \in \mathbb{R}^n$, $\displaystyle\sum_{\underline{k}\in\mathbb{Z}^n} \chi(\underline{u} - t_{\underline{k}}) = 1$;

($\chi 3$) For some $\beta > 0$,

$$m_{\beta,\Pi^n}(\chi) \;=\; \sup_{\underline{u}\in\mathbb{R}^n} \sum_{\underline{k}\in\mathbb{Z}^n} \left|\chi(\underline{u} - t_{\underline{k}})\right| \cdot \left\|\underline{u} - t_{\underline{k}}\right\|_2^{\beta} \;<\; +\infty,$$

where $\|\cdot\|_2$ denotes the usual Euclidean norm.

The linear multivariate sampling Kantorovich operators are defined by

$$(S_w f)(\underline{x}) \;:=\; \sum_{\underline{k}\in\mathbb{Z}^n} \chi(w\underline{x} - t_{\underline{k}}) \left[\frac{w^n}{A_{\underline{k}}} \int_{R^w_{\underline{k}}} f(\underline{u})\; d\underline{u}\right], \qquad (\underline{x}\in\mathbb{R}^n), \tag{1}$$

where $f : \mathbb{R}^n \to \mathbb{R}$ is a locally integrable function such that the above series is convergent for every $\underline{x}\in\mathbb{R}^n$,

$$R^w_{\underline{k}} \;:=\; \left[\frac{t_{k_1}}{w}, \frac{t_{k_1+1}}{w}\right] \times \left[\frac{t_{k_2}}{w}, \frac{t_{k_2+1}}{w}\right] \times ... \times \left[\frac{t_{k_n}}{w}, \frac{t_{k_n+1}}{w}\right],$$

$w > 0$ and $A_{\underline{k}} = \Delta_{k_1} \cdot \Delta_{k_2} \cdot ... \cdot \Delta_{k_n}$, $\underline{k}\in\mathbb{Z}^n$. In [19], the following approximation theorem has been proved, which shows the pointwise and uniform reconstruction of a multivariate signal or image by means of the above operators (1). This result is fundamental for the following applications developed in this paper.

Theorem 3.1. *Let $f : \mathbb{R}^n \to \mathbb{R}$ be a continuous and bounded function. Then, for every $\underline{x}\in\mathbb{R}^n$,*

$$\lim_{w\to+\infty} (S_w f)(\underline{x}) \;=\; f(\underline{x}).$$

In particular, if $f : \mathbb{R}^n \to \mathbb{R}$ is uniformly continuous and bounded, then

$$\lim_{w\to+\infty} \|S_w f - f\|_\infty \;=\; 0,$$

where $\|\cdot\|_\infty$ denotes the sup-norm, i.e., $\|f\|_\infty := \sup_{\underline{x}\in\mathbb{R}^n} |f(\underline{x})|$.

In general, the edges of visible images are sufficiently countered, which means to have jumps of the gray levels. From the mathematical point of view, this results in functions with discontinuities. Therefore, it is also important to have at disposal a theory which allows us to reconstruct not necessarily continuous signals. Hence, in order to obtain a reconstruction theorem for this kind of signals, we study the sampling Kantorovich operators in the general setting of Orlicz spaces.

First, we recall some basic notions concerning Orlicz spaces, see e.g. [37, 38].

The function $\varphi : \mathbb{R}_0^+ \to \mathbb{R}_0^+$ is said to be a φ-function if it satisfies the following assumptions:

($\varphi 1$) $\varphi(0) = 0$, $\varphi(u) > 0$ for every $u > 0$;

($\varphi 2$) φ is continuous and non decreasing on $\mathbb{R}_0^+$;

($\varphi 3$) $\lim_{u\to\infty} \varphi(u) \;=\; +\infty$.

For a fixed φ-function φ, one can consider the functional $I^\varphi : M(\mathbb{R}^n) \to [0, +\infty]$, where $M(\mathbb{R}^n)$ denotes the set of all measurable functions $f : \mathbb{R}^n \to \mathbb{R}$, of the form

$$I^\varphi[f] := \int_{\mathbb{R}^n} \varphi(|f(\underline{x})|)\; d\underline{x}, \qquad (f \in M(\mathbb{R}^n)).$$

The Orlicz space generated by φ is now defined by

$$L^{\varphi}(\mathbb{R}^n) := \{f \in M(\mathbb{R}^n) : \ I^{\varphi}[\lambda f] < \infty, \ \text{for some } \lambda > 0\}.$$

We can introduce in $L^{\varphi}(\mathbb{R}^n)$, a notion of convergence, called "modular convergence", which induces a topology (modular topology) on the space ([37, 38]). We will say that a net of functions $(f_w)_{w>0} \subset L^{\varphi}(\mathbb{R}^n)$ is modularly convergent to a function $f \in L^{\varphi}(\mathbb{R}^n)$ if

$$\lim_{w \to +\infty} I^{\varphi}[\lambda(f_w - f)] \ = \ 0,$$

for some $\lambda > 0$.

As a last basic property on Orlicz space, we recall that $C_c(\mathbb{R}^n)$, the set of all continuous functions having compact support, is modularly dense in $L^{\varphi}(\mathbb{R}^n)$, see [39].

For further results and details concerning Orlicz spaces, the readers can see [40, 41, 42, 43, 44, 45, 46].

Now, we recall the following continuity property for our operators with respect to the modular I^{φ}, useful to prove the modular convergence result for the family of sampling Kantorovich operators in $L^{\varphi}(\mathbb{R}^n)$.

Theorem 3.2. *Let φ be a convex φ-function. For every $f \in L^{\varphi}(\mathbb{R}^n)$ there holds*

$$I^{\varphi}[\lambda S_w f] \ \leq \ \frac{\|\chi\|_1}{\delta^n \cdot m_{0,\Pi^n}(\chi)} I^{\varphi}[\lambda m_{0,\Pi^n}(\chi) f],$$

for some $\lambda > 0$.
In particular, S_w maps $L^{\varphi}(\mathbb{R}^n)$ in $L^{\varphi}(\mathbb{R}^n)$.

The main modular convergence result in the setting of Orlicz spaces for the family (1) can be now formulated as follows.

Theorem 3.3. *Let φ be a convex φ-function. For every $f \in L^{\varphi}(\mathbb{R}^n)$, there exists $\lambda > 0$ such that*

$$\lim_{w \to +\infty} I^{\varphi}[\lambda(S_w f - f)] \ = \ 0.$$

For the sake of completeness we point out that the proof of Theorem 3.3 (see [19]) is based on the following fundamental steps:

1. the density of space $C_c(\mathbb{R}^n)$ in $L^{\varphi}(\mathbb{R}^n)$ with respect to the modular topology;
2. the modular continuity property for the operators S_w when f belongs to $L^{\varphi}(\mathbb{R}^n)$ (Theorem 3.2);
3. the modular convergence of the family of the operators S_w when f belongs to $C_c(\mathbb{R}^n)$ (which is a direct consequence of Theorem 3.1).

For further results concerning sampling Kantorovich operators, see e.g., [47, 48, 49, 50, 51, 52, 53, 54, 55].

The setting of Orlicz spaces allows us to give a unitary approach for the reconstruction since we may obtain convergence results for particular cases of Orlicz spaces.

For instance, choosing $\varphi(u) = u^p$, $1 \leq p < \infty$, we have that $L^{\varphi}(\mathbb{R}^n) = L^p(\mathbb{R}^n)$ and $I^{\varphi}[f] = \|f\|_p^p$, where $\|\cdot\|_p$ is the usual L^p-norm. Then, from Theorem 3.3 we obtain the following corollary.

Corollary 3.4. *For every $f \in L^p(\mathbb{R}^n)$, $1 \leq p < +\infty$,*

$$\lim_{w \to +\infty} \|S_w f - f\|_p \ = \ 0.$$

The corollary above, allows us to reconstruct L^p-signals (in L^p-sense), therefore signals/images not necessarily continuous.

Other examples of Orlicz spaces for which the above theory can be applied can be found e.g., in [18, 19, 37, 38, 40]. The theory of sampling Kantorovich operators in the general setting of Orlicz spaces allows us to obtain, by means of a unified treatment, several applications in many different contexts.

Finally, we show some examples of kernels used in order to define the multivariate sampling Kantorovich operators and for which the above results can be applied. For the sake of simplicity, from now on we consider the operators (1) in the case of a uniform sampling scheme, i.e., $t_{\underline{k}} = \underline{k}$, $\underline{k} \in \mathbb{Z}^n$.

As a first example, we can consider the univariate Fejér's kernel defined by

$$F(x) \ := \ \frac{1}{2}\mathrm{sinc}^2\left(\frac{x}{2}\right) \qquad (x \in \mathbb{R}),$$

where the *sinc*-function is given by

$$\mathrm{sinc}(x) \ := \ \begin{cases} \dfrac{\sin \pi x}{\pi x}, & x \in \mathbb{R} \setminus \{0\}, \\ 1, & x = 0. \end{cases}$$

We can define the multivariate Fejér's kernel by $\mathcal{F}_n(\underline{x}) = \prod_{i=1}^{n} F(x_i)$, $\underline{x} = (x_1, ..., x_n) \in \mathbb{R}^n$, which satisfies the conditions upon a multivariate kernel, see e.g. [19, 24, 55, 56]. Since Fejér's kernel $\mathcal{F}_n$ has unbounded support, one needs an infinite number of mean values $w^n \int_{R^w_{\underline{k}}} f(\underline{u})\, d\underline{u}$ in order to evaluate the corresponding sampling Kantorovich series at any given $\underline{x} \in \mathbb{R}^n$. If the function f has compact support, this problem does not arise, while, if the function has unbounded support, one can only take a finite number of these mean values into account, so the infinite sampling series must be truncated to a finite one, which leads to the so-called truncation error.

In order to avoid the truncation error, one can take kernels χ with bounded support.

Remarkable examples of kernels with compact support, can be constructed using the well-known univariate central B-spline of order $k \in \mathbb{N}$, defined by

$$M_k(x) := \ \frac{1}{(k-1)!} \sum_{i=0}^{k} (-1)^i \binom{k}{i} \left(\frac{k}{2} + x - i\right)_+^{k-1},$$

where the function $(x)_+ := \max\{x, 0\}$ denotes the positive part of $x \in \mathbb{R}$ (see [18, 19, 47]). The multivariate central B-spline kernel of order $k \in \mathbb{N}$ is defined by:

$$\mathcal{M}_k^n(\underline{x}) \ := \ \prod_{i=1}^{n} M_k(x_i), \qquad \underline{x} = (x_1, ..., x_n) \in \mathbb{R}^n,$$

and the functions $\mathcal{M}_k^n(\underline{x})$ satisfy all the conditions upon a multivariate kernel, see e.g. [19, 24, 55, 56].

Finally, other important examples of univariate kernels are given by the Jackson-type kernels, defined by

$$J_k(x) = c_k \operatorname{sinc}^{2k}\left(\frac{x}{2k\pi\alpha}\right), \quad x \in \mathbb{R},$$

with $k \in \mathbb{N}$, $\alpha \geq 1$, where the normalization coefficients c_k are given by

$$c_k := \left[\int_{\mathbb{R}} \operatorname{sinc}^{2k}\left(\frac{u}{2k\pi\alpha}\right) du\right]^{-1}.$$

The multivariate Jackson-type kernels, used in this paper for the reconstruction process, are defined by $\mathcal{J}_k^n(\underline{x}) := \prod_{i=1}^n J_k(x_i)$, $\underline{x} \in \mathbb{R}^n$; for more details, see e.g., [18, 36, 38, 57, 58]. For others useful examples of kernels, see e.g., [18, 57, 59, 60, 61, 62, 63].

3.1. Applications to Image Processing

In this section, we show how the multivariate sampling Kantorovich operators can be applied to reconstruct images, see [19, 56]. Every bi-dimensional gray scale image A (matrix) can be modeled as a step function I, with compact support, belonging to $L^p(\mathbb{R}^2)$, $1 \leq p < +\infty$. The most natural way to define I is:

$$I(x,y) := \sum_{i=1}^{m}\sum_{j=1}^{m} a_{ij} \cdot \mathbf{1}_{ij}(x,y), \quad (x,y) \in \mathbb{R}^2,$$

where $\mathbf{1}_{ij}(x,y)$, $i,j = 1,2,...,m$, are the characteristics functions of the sets $(i-1,\ i]\times(j-1,\ j]$ (i.e. $\mathbf{1}_{ij}(x,y) = 1$, for $(x,y) \in (i-1,\ i]\times(j-1,\ j]$ and $\mathbf{1}_{ij}(x,y) = 0$ otherwise). Note that the above function $I(x,y)$ is defined in such a way that, to every pixel (i,j) it is associated the corresponding grey level a_{ij}. Then, we can now consider the family of bivariate sampling Kantorovich operators $(S_w I)_{w>0}$ (for some kernel χ) that approximates I in L^p-sense. Now, in order to obtain a new image (matrix) that approximates the original one, it is sufficient to sample $S_w I$ (for some $w > 0$) with a fixed sampling rate. In particular, we can reconstruct the approximating images (matrices) taking into consideration different sampling rates and this is possible since we know the analytic expression of $S_w I$.

If the sampling rate is chosen higher than the original sampling rate, one can get a new image that has a better resolution than the original one's. The above procedure has been implemented by using MATLAB in order to obtain an algorithm based on the multivariate sampling Kantorovich theory. The pseudo-code of the proposed algorithm is shown in Table 1.

In the next sections, examples of thermographic images reconstructed by the sampling Kantorovich operators will be given to show the main applications of the theory to civil engineering.

4. Mechanical characteristics of masonry texture

The images obtained from thermography and enhanced by the reconstruction process by using the sampling Kantorovich algorithm, with a scaling factor $R > 1$, are used to estimate the elastic properties of the masonry taking into account the actual texture, achieving an appropriate description of the mechanical behavior.

In particular, the steps of the procedure that lead to the estimation of the elastic properties of the masonry starting from the (original or reconstructed) image are here briefly recalled and will be described in more details in the next sections. At first, the separation of the phases, with the

Objective: Reconstructing and improving the resolution of the original bivariate image I by sampling Kantorovich operators based upon the bivariate kernel χ.

Inputs: Original image I ($n \times n$ pixel resolution), the parameter $w > 0$ and the scaling factor R.

- Choice and definition of the kernel function χ.
- Definition of the size $(n \times R)\times(n \times R)$ of the reconstructed image.
- Computation of the matrices of the mean values (samples) of I by means of the Kronecker matrix product.
- Definition of the vectors containing the arguments of χ.

Iteration: Summation over $\underline{k}$ of all non-zero terms of the form $\chi(w\underline{x} - \underline{k}) \cdot \left[w^2 \int_{R^w_{\underline{k}}} I(\underline{u})\, d\underline{u}\right]$, for a suitable fixed grid of points $\underline{x}$.

Output: The reconstructed image with resolution $(n \times R)\times(n \times R)$.

Table 1: Pseudo-code of the sampling Kantorovich algorithm for image reconstruction.

identification of the stones and the mortar joints, is achieved by means of techniques belonging to the field of Digital Image Processing. The black-and-white image obtained is considered as a sample of the masonry and it is used to estimate the elastic properties by means of homogenization performed employing Finite Element Method; in particular, one finite element with appropriate mechanical characteristics (corresponding to that of the mortar or the stone) is assumed for each pixel; two kind of boundary conditions (essential and natural) are applied at the edge of the sample in order to evaluate the effective stiffness proprieties. From these, the elastic moduli are estimated assuming a mean isotropic behaviour of the masonry. Finally, the mechanical characteristics estimated for the masonries by means of the previous procedure is used in a finite element model of the building in order to estimate its modal properties (periods and modal shapes of vibration).

4.1. Separation of phases

The image is converted from gray-scale representation to black-and-white (binary) representation by means of techniques belonging to the field of Digital Image Processing (D.I.P.). The aim is to obtain a consistent separation of the phases, that is a correct identification of the pixel which belong to the blocks (bricks and/or stones) and those who belong to the matrix of mortar. In particular, after the conversion of the image in black-and-white, the areas consisting of white pixels are identified as blocks while the remaining areas of black pixels denotes the mortar joints. The method used to obtain the black-and-white image of the wall has been described in [64] and it is here briefly reminded.

At first, the gray-scale image is converted in binary by means of thresholding. The method proposed in [64] has been modified in order to compensate the effect of gradient of illumination in the original image. In fact, since the thermographic images are based on the measure of heat flux,

as described in detail previously, it is expected that, even if the material pattern is the same, the luminance gradient is not uniform. In particular the adaptive thresholding has been used (see [65]). The idea behind this approach is that, instead of computing a threshold using the information from the entire image, the threshold is evaluated using smaller portions of the image; these sub-images are likely to have an approximately uniform value of luminance. As a threshold, in the present case the mean value of gray level of each portion of the image has been used.

Thereafter, morphological operators are used to enhance the quality of the separation of the phases. In fact, the thresholding process generates an image which has several issues. In particular, salt-and-pepper noise would be erroneously interpreted, from a mechanical point of view, as either small portions of mortar inside the inclusions or very little stones inside mortar joints. Therefore the filling of the areas is performed in order to fix these issues. Moreover, erosion and dilation operators are applied in order to smooth the contours of the inclusions and to correct small defects still present in the image. It is worth noting that the morphological operators, besides the change of the boundaries of the inclusions, may change also the concentration of the phases, but this effect is generally small (in the order of few percent). Moreover, this difference is due to small stones scattered inside mortar joints, which are not real but due to thresholding process, and therefore it is correct to eliminate them from the image.

The image obtained is characterized by a consistent separation of phases, where each stone is surrounded by mortar joints and unrealistic conjunction of inclusions is avoided as much as possible.

An example of the results that can be obtained applying the previous method to both the original termographic image and to the image enhanced by means of sampling Kantorovich operators, built upon a Jackson type kernel, are shown in Fig. 1.

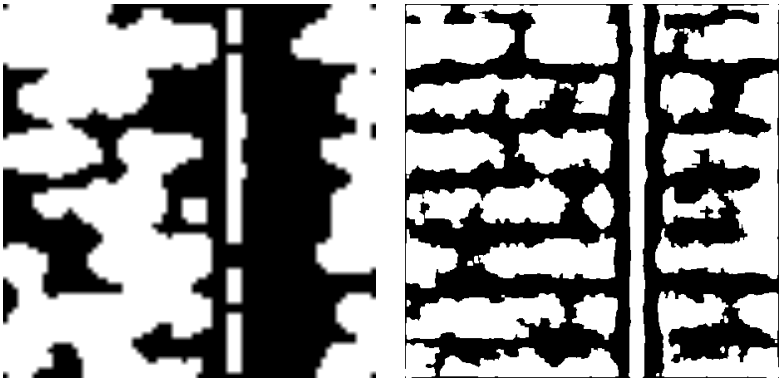

(a) (b)

Figure 1: (a) texture obtained using original thermographic image and (b) texture obtained using reconstructed image.

It is worth noting that between the original and the reconstructed thermographic images there are differences, other than in their resolution, also in their gray levels that greatly affects the estimation of the texture, which is our main interest: this is due to the threshold algorithm which operates in the range of gray levels which are modified and enhanced by the reconstruction process.

As can be observed, the elaboration of the original image generates unrealistic shape of the inclusion and irregular mortar joints (Fig. 1 (a)), while in the case of enhanced image the stones appear to be quite regular and, more meaningfully, the pattern is characterized by horizontal and non-aligned vertical mortar joints (Fig. 1 (b)). Moreover, the original image tends to overestimate

the percentage of mortar in the masonry. In fact, as a good building practice, the use of the mortar should be reduced as much as possible, only to allow a correct positioning of the inclusions (bricks and stones). This anomalous quantity of mortar affects the mechanical characteristics of the equivalent material, as will be shown in the following application to the case-study. Both these observations, together with the mathematical considerations previously discussed, lead us to conclude that the image reconstructed by means of sampling Kantorovich operators is more realistic, from an engineering point of view, than the original one.

4.2. Estimation of elastic properties

The masonry is an heterogeneous material with random micro-structure, given by the arrangement of blocks and mortar joints identified in the previous section. The knowledge of the particular arrangement for the masonry object of the analysis, i.e., the texture, allows the direct estimation of the mechanical parameters of a homogeneous material equivalent to the actual masonry. The equivalence is in the sense defined by [66]: when subjected to the same boundary conditions (b.c.), the overall response in terms of mean values of stresses and deformations of the heterogeneous material and of the equivalent homogeneous one is the same.

The procedure to estimate the elastic stiffness tensor, C, of the homogeneous equivalent material has been presented in [67] and here briefly reminded.

The stress tensor σ and the strain tensor ε are expressed using Voigt notation:

$$\sigma = \{\sigma_{xx}, \sigma_{yy}, \sigma_{zz}, \sigma_{yz}, \sigma_{xz}, \sigma_{xy}\}^T, \varepsilon = \{\varepsilon_{xx}, \varepsilon_{yy}, \varepsilon_{zz}, \varepsilon_{yz}, \varepsilon_{xz}, \varepsilon_{xy}\}^T. \tag{2}$$

The use of Voigt notation allows to express the stiffness 4th-order tensor C as a symmetric square matrix with 36 elements in the following way:

$$\sigma = C\,\varepsilon \tag{3}$$

The equivalence relation is given by:

$$\langle\sigma\rangle = C^{\mathrm{Hom}}\,\langle\varepsilon\rangle,$$

where $\langle\sigma\rangle$ and $\langle\varepsilon\rangle$ are the spatial average on the domain Ω of σ and ε, given by:

$$\langle\sigma\rangle = \frac{1}{|\Omega|}\int_\Omega \sigma\,\mathrm{d}\Omega, \quad \langle\varepsilon\rangle = \frac{1}{|\Omega|}\int_\Omega \varepsilon\,\mathrm{d}\Omega.$$

The stiffness elastic properties of the equivalent homogeneous material expressed by C^{Hom}, which accounts for the effective texture of the micro-structure, can be estimated by a suitable choice of boundary conditions. In general, if the domain Ω is not sufficiently large, the estimate of C^{Hom} depends on the b.c. applied. Two type of b.c. are mainly used: (i) essential boundary conditions, expressed in terms of displacements $u = \{u_x, u_y, u_z\}^T$, where the estimate of C^{Hom} is denoted by C^{E}; (ii) natural boundary conditions, expressed in terms of surface forces $f = \{f_x, f_y, f_z\}^T$, where the estimate of C^{Hom} is denoted by C^{N}. It is possible to prove (see [68]) that:

$$C^{\mathrm{N}} \leq C^{\mathrm{Hom}} \leq C^{\mathrm{E}},$$

where the order relation between two generic matrices X and Y expressed by $X \leq Y$ means that $z^T X\, z \leq z^T Y\, z$ for any non-null vector z.

The problem can be simplified if the hypothesis of plane-stress state are assumed, as it is usually true in the case of masonry walls. The plane-stress state is characterized by:

$$\sigma_{zz} = \sigma_{xz} = \sigma_{yz} = 0,$$

while the remaining components are only function of x and y, where x and y are coordinate axis lying in the plane of the wall.

In this case, the stress and strain tensors of (2) and the corresponding stiffness matrix of (3) are given by:

$$\sigma = \{\sigma_{xx}, \sigma_{yy}, \sigma_{xy}\}^T, \varepsilon = \{\varepsilon_{xx}, \varepsilon_{yy}, \varepsilon_{xy}\}^T \text{ and } C = \begin{bmatrix} C_{11} & C_{12} & C_{16} \\ C_{12} & C_{22} & C_{26} \\ C_{16} & C_{26} & C_{66} \end{bmatrix}. \tag{4}$$

and appropriate conditions at the boundary of the binary image concerning the portion analyzed are applied in order to estimate the tensor C in (4). In order to solve the boundary value problem, the Finite Element Method (F.E.M.) is used. In particular 4-node elements with plane stress formulation are used, assuming that each pixel of the binary image is a finite element.

In particular, the following boundary conditions are used:

- Essential boundary conditions allows to obtain a uniform value of $\varepsilon = \varepsilon^0$ over the domain of an homogeneous material, and consist of the following displacements:

$$u_x = \varepsilon^0_{xx} \cdot x + \varepsilon^0_{xy} \cdot y \tag{5a}$$
$$u_y = \varepsilon^0_{xy} \cdot x + \varepsilon^0_{yy} \cdot y \tag{5b}$$

  This allows to evaluate, by means of the F.E.M., the components of the stiffness matrix, C^{E}. For example, choosing $\varepsilon^0 = \{1, 0, 0\}^T$ and therefore adopting $u_x = x, u_y = 0$, the first column of C^{E} is given by $\{\langle\sigma_{xx}\rangle, \langle\sigma_{yy}\rangle, \langle\sigma_{xy}\rangle\}^T$, since $\{\langle\varepsilon_{xx}\rangle, \langle\varepsilon_{yy}\rangle, \langle\varepsilon_{xy}\rangle\}^T = \{1, 0, 0\}^T$ [68]. Similarly the second and third column of C^{E} can be obtained with $\varepsilon^0 = \{0, 1, 0\}^T$ and $\varepsilon^0 = \{0, 0, 1\}^T$ respectively.

- Natural boundary conditions allows to obtain a uniform value of $\sigma = \sigma^0$ over the domain of an homogeneous material, and consist of the following tractions:

$$f_x = \sigma^0_{xx} \cdot n_x + \sigma^0_{xy} \cdot n_y \tag{6a}$$
$$f_y = \sigma^0_{xy} \cdot n_x + \sigma^0_{yy} \cdot n_y \tag{6b}$$

  with n_x, n_y the direction cosines of the outer-pointing normal to the boundary, which allows to evaluate, by means of the F.E.M., the components of the inverse of stiffness matrix, $\left(C^{\mathrm{N}}\right)^{(-1)}$. For example, choosing $\sigma^0 = \{1, 0, 0\}^T$ and therefore adopting $f_x = n_x, f_y = 0$, the first column of $\left(C^{\mathrm{N}}\right)^{(-1)}$ is given by $\{\langle\varepsilon_{xx}\rangle, \langle\varepsilon_{yy}\rangle, \langle\varepsilon_{xy}\rangle\}^T$, since $\{\langle\sigma_{xx}\rangle, \langle\sigma_{yy}\rangle, \langle\sigma_{xy}\rangle\}^T = \{1, 0, 0\}^T$ [68]. Similarly the second and third column of $\left(C^{\mathrm{N}}\right)^{(-1)}$ can be obtained with $\sigma^0 = \{0, 1, 0\}^T$ and $\sigma^0 = \{0, 0, 1\}^T$ respectively.

In case that C^{E} and C^{N} are sufficiently close, C^{Hom} can be estimated through the following arithmetic mean (see [67]):

$$C^{\mathrm{Hom}} = \frac{1}{2}\left(C^{\mathrm{N}} + C^{\mathrm{E}}\right). \tag{7}$$

Since the behavior of the model is analyzed by means of modal analysis, in which the response to earthquake action is driven by lateral displacements, and low-rise building are considered, is possible to simplify the numerical analysis assuming the material is isotropic and a value of elastic moduli intermediate among those corresponding to horizontal and vertical directions have been used. The isotropic moduli can therefore be found through the components of the stiffness tensor C^{Hom} given by (7) by means of the following:

$$\nu = \frac{2\,C_{12}}{(C_{11} + C_{22})}, \tag{8a}$$

$$E = \frac{(C_{11} + C_{22})}{2}\left(1 - \nu^2\right), \tag{8b}$$

$$G = \frac{E}{2\,(1+\nu)}. \tag{8c}$$

The pseudo-code of the algorithm described in the present Section, that allows to find the relationship between the thermal image (original and reconstructed indifferently), the stiffness tensor and eventually the elastic isotropic moduli of the material, is shown in Table 2.

Once the mechanical characteristics of the masonry have been estimated by means of (8a), (8b), and (8c) using the proposed procedure, they can be used to model the building and perform the structural analysis.

5. Application to a case-study

The procedure presented in the previous section has been applied to a real-world case-study; it consists of a building located near Perugia, in central Italy.

The case-study is a typical detached country house of middle '60s. It consists of two levels and an attic and has a very simple architectural plan, consisting of a rectangle with sides 11 m and 11.4 m (see Fig. 2). The main front is eastward.

As usual for building of that age, the vertical structural elements consist in masonry walls. At first level the masonry walls have thickness of 40 cm and are made of rounded stones, while at the second level the masonry is made of squared tuff block and it has thickness of about 35 cm. The horizontal structural elements consist in mixed reinforce concrete/brick slabs (known as "SAP" in Italy) cast in a single direction. Both surfaces of the walls are plastered.

The loads acting on the building have been estimated according to the 2008 Italian Building Code [69]. In particular, the building is placed in a medium risk seismic area, with an expected peak ground acceleration for a 475-year mean return period earthquake of 0.161 g.

According to a preliminary visual survey, the structure does not have strong asymmetry between principal directions and, the distribution of the masses is quite uniform.

The aim of the following sections is to investigate the enhancement in the understanding of structural behavior which may be achieved by means of thermographic survey. All the models described in the following have been analyzed by means of F.E.M. using a commercial code, and

Objective: Estimating the isotropic elastic moduli E and ν of the masonry.

Inputs: Original or reconstructed thermographic image I ($n \times n$ pixel resolution) of the masonry.

- Separation of the phases by means of thresholding.
- Application of morphological operators to correct the issues due to the thresholding and to obtain a sample of the masonry with consistent position of stones and mortar joints.
- Modeling of the sample by means of Finite Element Method.
  Each pixel is a 4-node Finite Element with stone's or mortar's mechanical characteristics.
  The model consists of $n \times n$ finite elements.
- Application of essential boundary conditions and estimation of C^E.
  At each node on the boundary of the model the displacements are applied according to (5a) and (5b). First, second and third column of C^E are obtained using $\varepsilon^0 = \{1,0,0\}^T$, $\varepsilon^0 = \{0,1,0\}^T$ and $\varepsilon^0 = \{0,0,1\}^T$ respectively.
- Application of natural boundary conditions and estimation of C^N.
  At each node on the boundary of the model the forces are applied according to (6a) and (6b). First, second and third column of $\left(C^N\right)^{(-1)}$ are obtained using $\sigma^0 = \{1,0,0\}^T$, $\sigma^0 = \{0,1,0\}^T$ and $\sigma^0 = \{0,0,1\}^T$ respectively.
- Estimation of the effective stiffness tensor C^{Hom}:
$$C^{\mathrm{Hom}} = \tfrac{1}{2}\left(C^{\mathrm{E}} + C^{\mathrm{N}}\right)$$
- Estimation of the isotropic elastic moduli E, ν and G:
$$\nu = \tfrac{2\,C_{12}}{(C_{11}+C_{22})}, E = \tfrac{(C_{11}+C_{22})}{2}\left(1-\nu^2\right), G = \tfrac{E}{2\,(1+\nu)}.$$

Iteration: Repeat for each different texture of masonry present in the building.

Output: The values of E, ν and G that can be used as elastic characteristics of the masonries in a finite element model of the whole building.

Table 2: Pseudo-code of the algorithm that allows to find the relationship between the thermal image (original and reconstructed) and the elastic isotropic moduli of the masonry.

employing finite elements of shell type made of material with isotropic behaviour to model masonry walls.

The first model is constructed using information that can be gathered by the visual survey only.

In a second model, the information concerning the actual geometry of vertical structural elements acquired by means of thermographic survey have been used. In particular a rather strong reduction in resisting section of the main front walls due to a partial filling of the openings has been detected (see Fig. 3).

In the third model, also information about the actual texture of masonries of each level, as

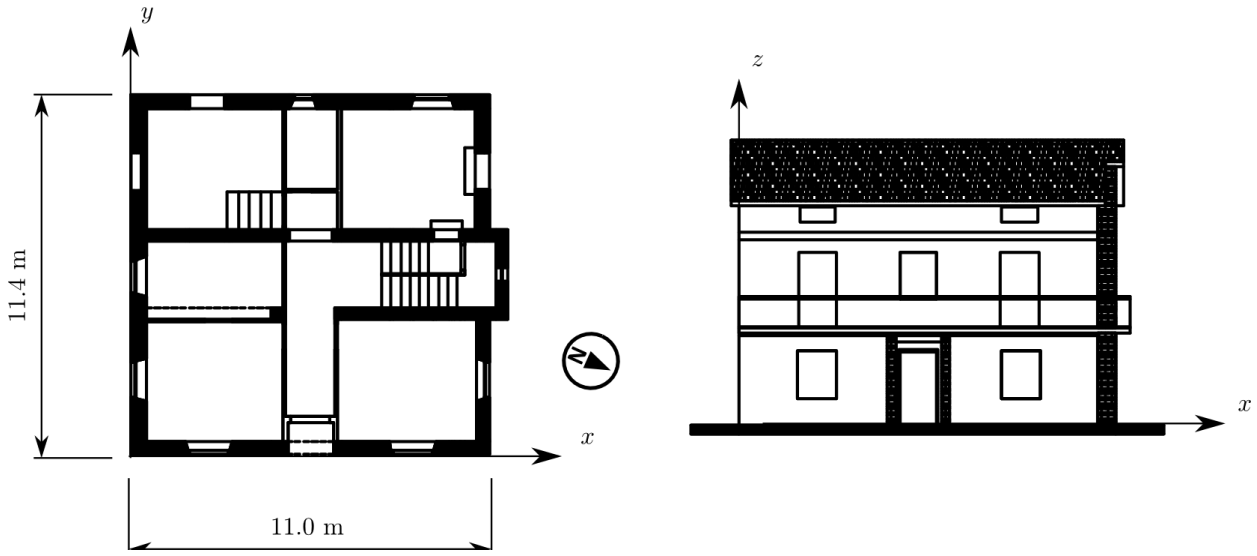

Figure 2: Plan and east front of case-study building.

Figure 3: View of east front in visible (left) and infrared (right) range.

can estimated from the analysis of reconstructed images, have been used. In particular, from the thermographic images taken on the south front, two portions of masonry were extracted: one belonging to ground level, which is made of chaotic masonry, and the other from second level, which consists of almost periodic masonry (Fig. 4).

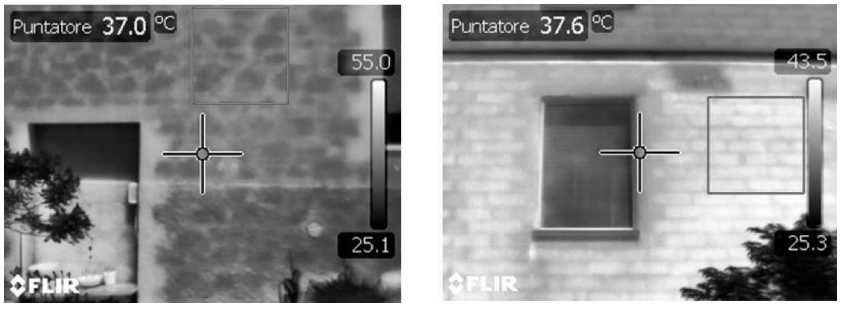

Figure 4: Portion of masonries analyzed in south front: chaotic masonry of ground level (left) and periodic masonry of second level (right).

The schematic succession of the models is depicted in Fig. 5.

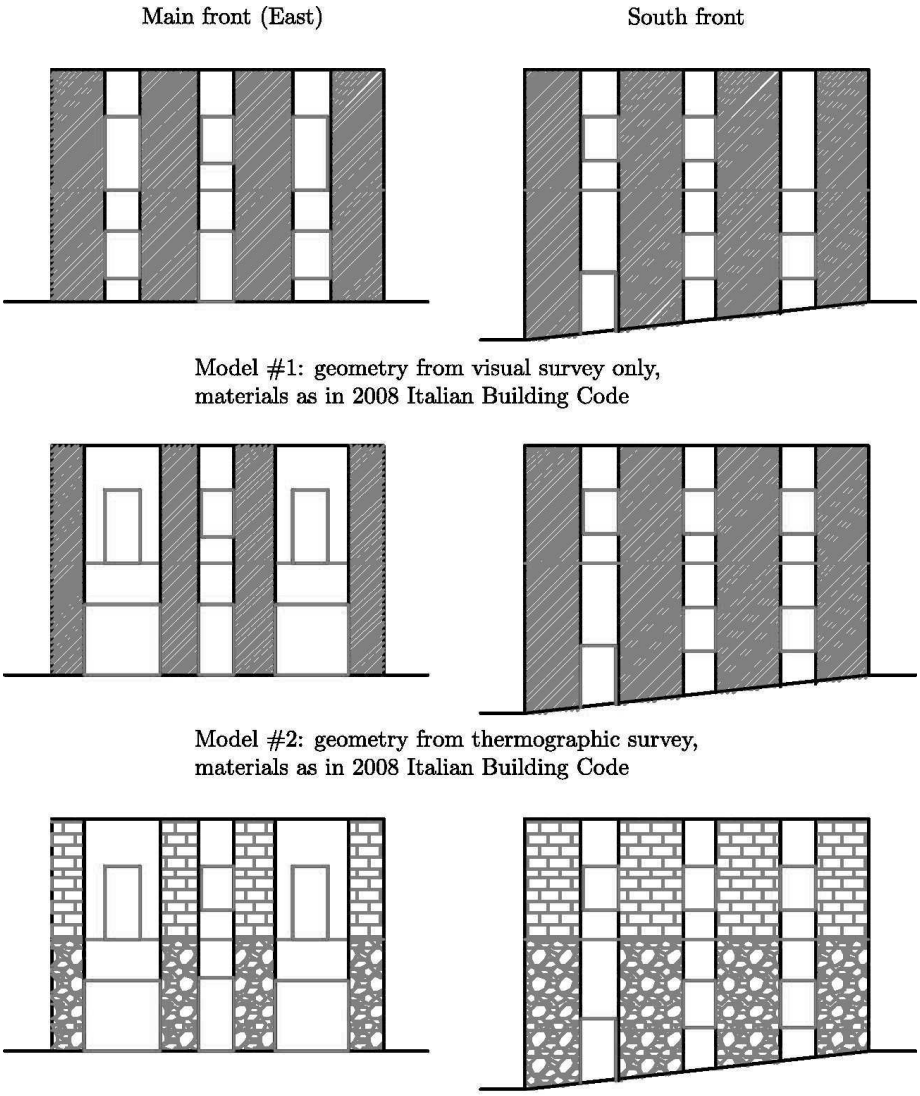

Figure 5: Schematic description of three models.

The behavior under seismic actions can be estimated by means of response spectrum modal analysis, which is the approach suggested by the Code. The main advantage of this approach is that the structure is modeled by means of multiple elementary oscillators for which the response to the earthquake action can be easily estimated. In this kind of analysis, the period and the shape of each mode greatly influence the response. In particular the shifting in the period may increase or decrease the modal acceleration and therefore the force distribution in the mode. As a rule-of-thumb, the periods tend to increase as the mass involved in each mode increases and as the elastic modulus of the materials decreases. Moreover, the presence of a significant torsional component coupled with each translation mode could contribute to increase the internal forces in

the structural elements. Finally, the distribution of the mass among the modes, expressed by means of mass participating ratio, is also important since the seismic force is proportional both to modal acceleration and to modal mass.
The effect of the previous factors will be discussed in detail for each of the models.

Model #1

The geometry of the vertical structural elements has been obtained by means of a visual survey. As previously stated, the first level masonry is made by stones and mortar, while the second level masonry is made by tuff bricks and mortar. In both cases the mortar joints thickness is of the order of 5–10 mm.

The mechanical characteristics (Young's modulus E, shear modulus G, Poisson ratio ν, weight W) used for the materials of both levels are reported in Tab. 3. In particular, for the first level the values of the masonry classified as "split stone masonry with good texture" have been used, adopting for E and G the superior of the ranges (1500–1980 MPa and 500–660 MPa respectively) suggested by the code, since the masonry is quite recent and still in good conditions, and adopting the factors due to the use of mortar with good mechanical characteristics, 1.3, and the presence of transverse connection, 1.3. For the second level the values of the masonry classified as "soft stone (tuff, etc.) ashlar masonry" have been used, adopting for E and G the mean of the ranges (900–1260 MPa and 300–420 MPa respectively) suggested by the code due to the quality of the tuff found in Central Italy which is a low/medium strength one (see, for example, table in [70]), and adopting the factor due to the use of mortar with good mechanical characteristics, 1.5.

	E	G	W
	$\mathrm{N\,mm^{-2}}$	$\mathrm{N\,mm^{-2}}$	$\mathrm{kN\,m^{-3}}$
first level	3346	1115	20.0
second level	1620	540	16.0

Table 3: Mechanical characteristics in Model #1.

Model #2

The thermographic survey has been used to obtain detailed information about the actual geometry of masonry walls. In general the survey may reveal:

- the existence of openings which have been filled and subsequently hidden by the plaster;
- the reduction of the dimensions of an opening by partial filling.

In particular, the survey has shown that the openings of the ground level of the main front have been partially filled, and therefore the structural dimensions of the adjacent walls have to be greatly reduced. This in turn compels to reduce also the dimensions of the openings at the second level, and therefore the contribution to the overall stiffness of the front is reduced.

It is worth noting that the revealing of a completely filled opening at the second level in the south front is not very significant since it is aligned with the opening at ground level and therefore does not modify the width of masonry walls.

The same mechanical characteristics for masonries used in Model #1 and reported in Tab. 3, have been used.

Model #3

In the last model, the geometry of the masonry walls is the same used for Model #2. Anyway, the information obtained by the study of the actual texture of masonries at first and second level, as shown in Fig. 4, have been used.

The images relative to these portions were enhanced by means of the reconstruction method based on sampling Kantorovich operators, using a scale factor $R = 6$, and afterwards the elastic characteristics of an homogeneous equivalent material were estimated. Anyway, the weight was assumed equal to the values suggested by the code. The results are reported in the following, together with those obtained using non reconstructed images, to make a comparison.

Chaotic masonry

The image reconstructed by means of sampling Kantorovich operators together with its black and white version obtained by D.I.P. (which make up the texture algorithm) of the sample of chaotic masonry is shown in Fig. 6 (a) and (b).

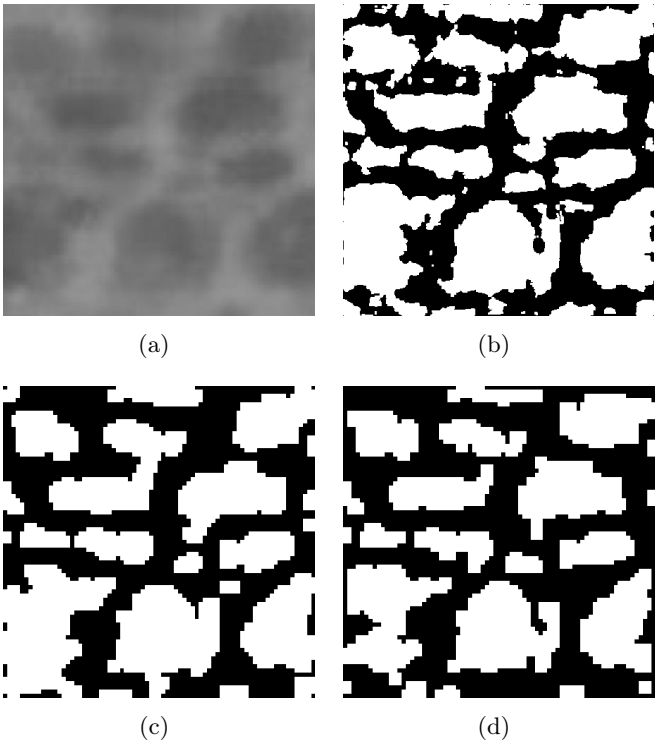

Figure 6: Images of chaotic masonry sample: (a) reconstruction by sampling Kantorovich operators, (b) texture of the reconstructed image, (c) texture of the original (non reconstructed) image, (d) texture of the original (non reconstructed) image obtained using a smaller window for adaptive thresholding.

It was assumed that the constituent phases have the mechanical characteristics reported in Tab. 4. The Young's modulus, E, and the Poisson's coefficient, ν, have been estimated employing values commonly found in literature. In particular, a value of $E = 25000\,\text{MPa}$ was assumed for natural stone, which, considering a strength to Young's modulus ratio of 300 (see, for example, [71]), corresponds to a compressive strength slightly larger than 80 MPa, coherent to that of a medium-strength limestone. The Young's modulus of mortar has been estimated assuming a strength to

	E	ν
	$\mathrm{N\,mm^{-2}}$	
block (natural stone)	25000	0.20
mortar (M2.5)	2500	0.20

Table 4: Mechanical characteristics of components of chaotic masonry.

Young's modulus ratio of 1000 as suggested for the masonry by the Italian Building Code [69]. Moreover, the focus of the paper is on the proposal of a procedure which could be applied in the analysis of the vulnerability of existing buildings, and not in the specific values for the case at hand. Anyway, some considerations on the influence of the Young's moduli of the phases on the estimated homogeneous values for the masonry are reported at the end of this section.

The stiffness matrices C^{N}, C^{E} and C^{Hom} estimated by means of the procedure previously described are:

$$C^{\mathrm{N}} = \begin{bmatrix} 7419 & 1381 & 0 \\ 1381 & 6426 & 0 \\ 0 & 0 & 2482 \end{bmatrix},$$

$$C^{\mathrm{E}} = \begin{bmatrix} 8200 & 1429 & 0 \\ 1429 & 7233 & 0 \\ 0 & 0 & 2850 \end{bmatrix},$$

$$C^{\mathrm{Hom}} = \begin{bmatrix} 7809 & 1405 & 0 \\ 1405 & 6830 & 0 \\ 0 & 0 & 2666 \end{bmatrix}.$$

Even if the values of C^{N} are quite far from those of C^{E}, and it is known that the estimation of the equivalent material benefit of an increasing of the sample dimensions, it was assumed that the values of C^{Hom} obtained, can be a good estimator C of the equivalent homogeneous material. As can be appreciated, the equivalent homogeneous material has orthotropic behavior.

For comparison, the results obtained using the non reconstructed image, shown in Fig. 6(c), are also reported:

$$\widetilde{C}^{\mathrm{Hom}} = \begin{bmatrix} 7013 & 1290 & 0 \\ 1290 & 6589 & 0 \\ 0 & 0 & 2563 \end{bmatrix}.$$

The difference seems to be mainly due to different concentration of phases, in particular in the non reconstructed image the percentage of area occupied by stones is about 51.1 %, while in the reconstructed image it is about 55.4 %. In general, the equivalent elastic modulus is an increasing function of the percentage of stones (which is stiffer).

In this sense, the reconstructed image is better than the original one since, from an engineering point of view, is reasonable that the builder try to minimize the use of mortar employing a joint thickness as small as possible to connect all the stones.

Moreover, the possibility of using the original, non reconstructed, image adopting a smaller window for the adaptive thresholding has been considered. The resulting texture is shown in Fig. 6(d): as can be appreciated, some of the smaller stones have disappeared. This is confirmed

by the evaluation of $\widetilde{C}^{\mathrm{Hom}}$:

$$\widetilde{C}^{\mathrm{Hom}} = \begin{bmatrix} 6436 & 1138 & 0 \\ 1138 & 5627 & 0 \\ 0 & 0 & 2195 \end{bmatrix},$$

where, as previously noted, the difference seems to be mainly due to different concentration of phases, which passes from 55.4 % in the reconstructed image to 47.0 % of the present case. Therefore, simply reducing the size of window to be used in the adaptive thresholding do not bring to reasonable results.

The obtained values of the mechanical characteristics E and G of the homogeneous equivalent material are reported in Tab. 5.

	E $\mathrm{N\,mm^{-2}}$	G $\mathrm{N\,mm^{-2}}$	W $\mathrm{kN\,m^{-3}}$
reconstructed image	7050	2957	20.0
non reconstructed image	6556	2756	20.0

Table 5: Mechanical characteristics of chaotic masonry in Model #3.

In the case of chaotic masonry a study of the sensitiveness of equivalent homogeneous parameters to mechanical parameters of the constituent phases has been made. The results, obtained using the reconstructed image, are reported in Tab. 6.

		E_{block}		
		20000	25000	30000
E_{mortar}	2000	5640	6063	6412
	2500	6530	7050	7481
	3000	7333	7949	8459

Table 6: Modulus of Young of the equivalent homogeneous material corresponding to different Young's moduli of constituent phases.

As can be appreciated, the error which is made using a non reconstructed image instead of a reconstructed one is of the same order as a 20% error on the stones' elastic modulus, as shown in Tab. 6. Therefore, even if the elastic moduli of the phases should be known with sufficiently accuracy, for example by means of non-destructive methods as drilling test and rebound hammer, using a non reconstructed image may nevertheless lead to significant errors on the estimation of equivalent elastic moduli. This confirm the convenience of using image reconstruction in the estimation of mechanical characteristics of masonry textures.

Periodic masonry

The image reconstructed by means of sampling Kantorovich operators together with its black and white version obtained by D.I.P. (texture algorithm) of the sample of periodic masonry is shown in Fig. 7.

It was assumed that the constituent phases have the mechanical characteristics reported in Tab. 7. The Young's modulus, E, of tuff has been chosen according to values reported in [70] and valid for material found in Orvieto zone, which is nearby the location of the case-study building.

The stiffness matrices C^{N}, C^{E} and C^{Hom} are:

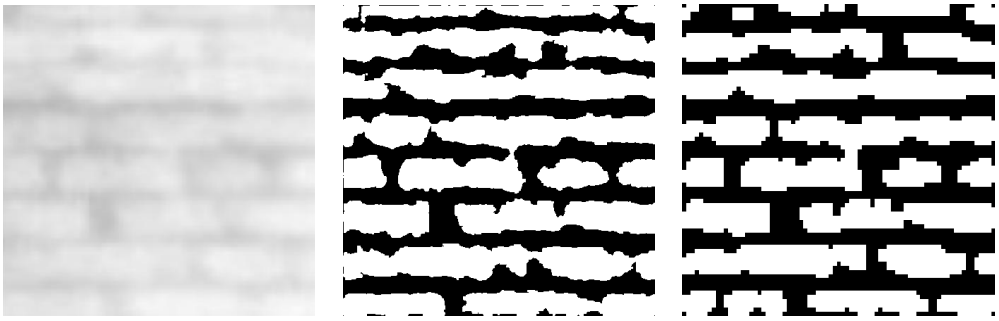

(a) (b) (c)

Figure 7: Images of periodic masonry sample: (a) reconstruction by sampling-Kantorovich operators, (b) texture of the reconstructed image, (c) texture of the original (non reconstructed) image.

	E	ν
	$\mathrm{N\,mm^{-2}}$	
block (tuff)	1700	0.20
mortar (M2.5)	2500	0.20

Table 7: Mechanical characteristics of components of periodic masonry.

$$C^{\mathrm{N}} = \begin{bmatrix} 2099 & 412 & 0 \\ 412 & 2053 & 0 \\ 0 & 0 & 821 \end{bmatrix},$$

$$C^{\mathrm{E}} = \begin{bmatrix} 2105 & 413 & 0 \\ 413 & 2056 & 0 \\ 0 & 0 & 823 \end{bmatrix},$$

$$C^{\mathrm{Hom}} = \begin{bmatrix} 2102 & 412 & 0 \\ 412 & 2054 & 0 \\ 0 & 0 & 822 \end{bmatrix}.$$

As can be appreciated, the equivalent homogeneous material has a mechanical behavior which is almost isotropic. Moreover the values of C^{N} and C^{E} are very close, so it can be assumed that Hill's criterion is satisfied.

For comparison, the results obtained using the non reconstructed image, shown in Fig. 7(c), are also reported:

$$\widetilde{C}^{\mathrm{Hom}} = \begin{bmatrix} 2136 & 419 & 0 \\ 419 & 2091 & 0 \\ 0 & 0 & 837 \end{bmatrix}.$$

In this case, the percentage of area occupied by stones of the non reconstructed image is about 53.7 %, while that one of the reconstructed image is about 58 %; also in this case the rising of the percentage of the stiffer phase (which in this case is the mortar) increases the equivalent elastic moduli. Nevertheless, the effect of reconstruction is less important than in the case of chaotic masonry, which is therefore more sensible to the the correct assessment of the texture.

The obtained values of equivalent mechanical properties are reported in Tab. 8.

E	G	W
$\mathrm{N\,mm^{-2}}$	$\mathrm{N\,mm^{-2}}$	$\mathrm{kN\,m^{-3}}$
1996	833	16.0

Table 8: Mechanical characteristics of periodic masonry in Model #3.

5.1. Comparison of results and discussion

In Tab. 9 the periods of the first three modes are reported. For all the models, the first mode is in East–West direction, along the y axis, the second is in North–South direction, along the x axis, and the third is mainly torsional. Anyway, the second mode is not a pure translational one since the asymmetry in the walls distribution adds to the mode a torsional component.

	T_1	T_2	T_3
	s	s	s
Model #1	0.22	0.15	0.13
Model #2	0.22	0.14	0.13
Model #3	0.18	0.13	0.11

Table 9: Periods of the first three modes.

As can be noted, the first two models have the same period for the fundamental mode in y direction; nevertheless, in x direction there is a slight difference due to the reduction on masonry walls width discovered by means of thermographic survey.

The periods of third model show a reduction of about 30%, this was expected since even if the geometry is the same of the second model, the homogenization gave greater value of equivalent elastic moduli.

An important issue which is addressed by the Code is torsional deformability, expressed by the ratio $r_{\min}/l_s$, where $r_{\min}$ is the minimum radius of gyration and l_s is the polar inertia radius. The Code state that if the ratio is lower than 0.8 the structure is torsionally deformable, and therefore special caution has to be used and possibly the distribution of the masses and/or the distribution of structural elements should be modified.

The value of $r_{\min}/l_s$ is reported in Tab. 10.

	$r_{\min}/l_s$
Model #1	1.082
Model #2	1.068
Model #3	1.059

Table 10: Torsional deformability of three models.

It can be noted that all the models have value of $r_{\min}/l_s > 0.8$, and therefore they are not torsionally deformable. Anyway, both the reduction of masonry walls width in main front and the increasing in the value of elastic moduli tend to decrease the value of $r_{\min}/l_s$ and therefore to increase the sensitivity to torsional deformation.

Finally, the mass participating ratio of the first three modes, indicated with M_1, M_2 and M_3, for the two principal direction of seismic action is shown in Tab. 11.

	Seismic action along x			Seismic action along y		
	M_1	M_2	M_3	M_1	M_2	M_3
Model #1	0.00	0.64	0.13	0.73	0.00	0.00
Model #2	0.00	0.51	0.27	0.73	0.01	0.00
Model #3	0.00	0.46	0.26	0.68	0.01	0.00

Table 11: Mass participating ratio of the first three modes for two direction of seismic action.

As already discussed previously, for seismic action in x direction the structure response is dominated by second mode, which is a coupled torsional/flexural mode; for seismic action in y direction the response is dominated by first mode, which is almost pure flexural.

It is also worth noting that Model #3 shows a reduced mass participating ratio for the fundamental mode in each direction, and therefore a greater number of modes should be considered in the evaluation of seismic response in order to achieve a suitable accuracy.

6. Concluding remarks

Starting from thermographic images of portions of masonry walls, the reconstruction process by means of the sampling Kantorovich operators allowed to increase their resolution and therefore it was possible to estimate the mechanical characteristics (Young's modulus and shear modulus) of homogeneous materials equivalent to actual masonries, taking into account the texture (i.e., the arrangement of blocks and mortar joints). These materials were used to model the behavior of a case study under seismic action. Moreover, the same thermographic survey that allowed to investigate the texture of the masonries was also used to detect the actual geometry of masonry walls, enhancing the quality of the model with respect to that based on visual survey only.
In particular the proposed approach suggests a procedure to overcome some difficulties that arise when dealing with the vulnerability analysis of existing structures, which are: i) the knowledge of the actual geometry of the walls (in particular the identification of hidden doors and windows); ii) the identification of the actual texture of the masonry and the distribution of inclusions and mortar joints, and from this iii) the estimation of the elastic characteristics of the masonry. It is noteworthy that, for item i) the engineer has limited knowledge, due to the lack of documentation, while for items ii) and iii) he usually use tables proposed in technical manuals and standards which however give large bounds in order to encompass the generality of the real masonries. Therefore by means of a single thermographic survey, together with the methods previously proposed, it is possible to gather information about all these three critical items.

Moreover, it has been shown that the uncertainties due to the lack of knowledge of the exact texture are of the same order of those due to an insufficient mechanical characterization of the constituent phases, and therefore the use of reconstruction techniques on thermographic images is useful to avoid an excessive approximation on the estimation of equivalent mechanical characteristics of the masonry. It is worth noting that, while the experimental estimation of the Young's modulus of an existing masonry usually requires rather invasive tests (such as double flat-jack tests), using the proposed procedure (operating on thermographic images reconstructed by means of sampling Kantorovich operators which are used to estimate the equivalent elastic moduli on the base of the actual texture) it is sufficient to estimate the mechanical characteristics of the constituent phases with non-destructive tests (such as, for example, drilling test and/or rebound hammer).

Acknowledgments

The authors wish to thank the Reviewers for their careful and insightful comments which permitted to enhance the quality of the paper.

References
References

[1] D.J. Titman, *Applications of thermography in non-destructive testing of structures*, NDT & E International, **34** (2) (2001), 149–154.

[2] Y.Y. Hung, Y.S. Chen, S.P. Ng, L. Liu, Y.H. Huang, B.L. Luk, R.W.L. Ip, C.M.L. Wu, P.S. Chung, *Review and comparison of shearography and active thermography for nondestructive evaluation*, Materials Science and Engineering: R: Reports, **64** (5-6) (2009), 73–112.

[3] R. W. Arndt, *Square pulse thermography in frequency domain as adaptation of pulsed phase thermography for qualitative and quantitative applications in cultural heritage and civil engineering*, Infrared Physics & Technology, **43** (4) (2010), 246–253.

[4] D.M McCann, M.C Forde, *Review of NDT methods in the assessment of concrete and masonry structures*, NDT & E International, **34** (2) (2001), 71–84.

[5] Rao, D. S. Prakashn, *Infrared thermography and its applications in civil engineering*, The Indian Concrete Journal, May 2008 (2008), 41–50.

[6] A. Hoyano, K. Asano, T. Kanamaru, *Analysis of the sensible heat flux from the exterior surface of buildings using time sequential thermography*, Atmospheric Environment, **33** (24-25) (1999), 3941–3951.

[7] T. Astarita, G. Cardone, G.M. Carlomagno, *Infrared thermography: An optical method in heat transfer and fluid flow visualisation*, Optics and Lasers in Engineering, **44** (3-4) (2006), 261–281.

[8] H. Wiggenhauser, *Active IR-applications in civil engineering*, Infrared Physics & Technology, **43** (2002), 233–238.

[9] S. Bhalla, S. Tuli, R. Arora, *Defect detection in concrete structures using thermal imaging techniques*, Experimental Techniques, **35** (4) (2011), 39–43.

[10] M.R Clark, D.M McCann, M.C Forde, *Application of infrared thermography to the non-destructive testing of concrete and masonry bridges*, NDT & E International, **36** (4) (2003), 265–275.

[11] C. Meola, *Infrared thermography of masonry structures*, Infrared Physics & Technology, **49** (3) (2007), 228–233.

[12] N.P Avdelidis, A Moropoulou, *Applications of infrared thermography for the investigation of historic structures* Journal of Cultural Heritage, **5** (1) (2004), 1296–2074.

[13] C. Ibarra-Castanedo, D. GonzÃąlez, M. Klein, M. Pilla, S. Vallerand, X. Maldague, *Infrared image processing and data analysis*, Infrared Physics & Technology, **46** (1-2) (2004), 75–83.

[14] C. Ni, Q. Li, L. Z. Xia, *A novel method of infrared image denoising and edge enhancement*, Signal Processing, **88** (6) (2008), 1606–1614.

[15] S. D. Holland, J. Renshaw, *Physics-based image enhancement for infrared thermography*, NDT & E International, **43** (5) (2010), 440–445.

[16] X. Bai, F. Zhou, B. Xue, *Infrared image enhancement through contrast enhancement by using multiscale new top-hat transform*, Infrared Physics & Technology, **54** (2) (2011), 61–69.

[17] T. Astarita, G. Cardone, G.M. Carlomagno, C. Meola, *A survey on infrared thermography for convective heat transfer measurements*, Optics & Laser Technology, **32** (2000), 593–610

[18] C. Bardaro, P.L. Butzer, R.L. Stens, G. Vinti, *Kantorovich-Type Generalized Sampling Series in the Setting of Orlicz Spaces*, Sampling Theory in Signal and Image Processing, **6** (1) (2007), 29–52.

[19] D. Costarelli, G. Vinti, *Approximation by Multivariate Generalized Sampling Kantorovich Operators in the Setting of Orlicz Spaces*, Bollettino U.M.I., Special volume dedicated to Prof. Giovanni Prodi, (9) **IV** (2011), 445–468.

[20] P.L. Butzer, *A survey of the Whittaker-Shannon sampling theorem and some of its extensions*, Journal of Mathematical Research and Exposition, **3** (1983), 185–212.

[21] P.L. Butzer, S. Ries, R.L. Stens, *Shannon's sampling theorem, Cauchy's integral formula, and related results*, In: Anniversary Volume on Approximation Theory and Functional Analysis, (Proc. Conf., Math. Res. Inst. Oberwolfach, Black Forest, July 30-August 6, 1983), P.L. Butzer, R.L. Stens and B.Sz.-Nagy (Eds.), Internat. Schriftenreihe Numer. Math. **65**, Birkhäuser, Basel, 1984, 363–377.

[22] S. Ries, R.L. Stens, *Approximation by generalized sampling series,* Constructive Theory of Functions'84, Sofia, 1984, 746–756.
[23] P.L. Butzer, S. Ries, R.L. Stens, *Approximation of continuous and discountinuous functions by generalized sampling series*, Journal of Approximation Theory, **50** (1987), 25–39.
[24] P.L. Butzer, A. Fisher, R.L. Stens, *Generalized sampling approximation of multivariate signals: theory and applications*, Note di Matematica, **10**, Suppl. n. 1 (1990), 173–191.
[25] P.L. Butzer, R.L. Stens, *Sampling theory for not necessarily band-limited functions: a historical overview,* SIAM Review, **34** (1) (1992), 40–53.
[26] P.L. Butzer, R.L. Stens, *Linear prediction by samples from the past*, Advanced Topics in Shannon Sampling and Interpolation Theory, (editor R.J. Marks II), Springer-Verlag, New York, 1993.
[27] C. Bardaro, G. Vinti, *A general approach to the convergence theorems of generalized sampling series,* Applicable Analysis, **64** (1997), 203–217.
[28] G. Vinti, *A general approximation result for nonlinear integral operators and applications to signal processing*, Applicable Analysis, 79 (2001), 217–238.
[29] C. Bardaro, G. Vinti, *An Abstract Approach to Sampling Type Operators Inspired by the Work of P.L. Butzer - Part I - Linear Operators*, Sampling Theory in Signal and Image Processing, **2** (3) (2003), 271–296.
[30] G. Vinti, *Approximation in Orlicz spaces for linear integral operators and Applications*, Rendiconti del Circolo Matematico di Palermo, Serie II, 76 (2005), 103–127.
[31] C. Bardaro, P.L. Butzer, R.L. Stens, G. Vinti, *Prediction by samples from the past with error estimates covering discontinuous signals*, IEEE, Transaction on Information Theory, **56** (1) (2010), 614–633.
[32] C. Bardaro, I. Mantellini, R.L. Stens, J. Vautz, G. Vinti, *Generalized sampling approximation for multivariate discontinuous signals and application to image processing*, in print in: New Perspectives on Approximation and Sampling Theory-Festschrift in honor of Paul Butzer's 85th birthday, Birkhauser (2014).
[33] A.J. Jerry, *The Shannon sampling-its various extensions and applications: a tutorial review*, Proc. IEEE, **65** (1977), 1565–1596.
[34] L. Bezuglaya, V. Katsnelson, *The sampling theorem for functions with limited multi-band spectrum I*, Zeitschrift für Analysis und ihre Anwendungen, **12** (1993), 511–534.
[35] L. Angeloni, G. Vinti, *Rate of approximation for nonlinear integral operators with applications to signal processing*, Differential and Integral Equations, **18** (8) (2005), 855–890.
[36] C. Bardaro, P.L. Butzer, R.L. Stens, G. Vinti, *Approximation of the Whittaker Sampling Series in terms of an Average Modulus of Smoothness covering Discontinuous Signals*, Journal of Mathematical Analysis and Applications, **316** (2006), 269–306.
[37] J. Musielak, *Orlicz Spaces and Modular Spaces*, Springer-Verlag, Lecture Notes in Math. **1034**, 1983.
[38] C. Bardaro, J. Musielak - G. Vinti, *Nonlinear Integral Operators and Applications,* De Gruyter Series in Nonlinear Analysis and Applications, New York, Berlin, **9**, 2003.
[39] C. Bardaro, I. Mantellini, *Modular Approximation by Sequences of Nonlinear Integral Operators in Musielak-Orlicz Spaces*, Atti Sem. Mat. Fis. Univ. Modena, special issue dedicated to Professor Calogero Vinti, suppl. vol. 46, (1998), 403–425.
[40] J. Musielak, W. Orlicz, *On modular spaces,* Studia Mathematica, **28** (1959), 49–65.
[41] M.A. Krasnosel'skiĭ, Ya.B. Rutickiĭ, *Convex Functions and Orlicz Spaces*, P. Noordhoff Ltd. - Groningen - The Netherlands, 1961.
[42] W.M. Kozlowski, *Modular Function Spaces*, (Pure Appl. Math.) Marcel Dekker, New York and Basel, 1988.
[43] L. Maligranda, *Orlicz Spaces and Interpolation*, Seminarios de Matematica, IMECC, Campinas, 1989.
[44] M.M. Rao, Z.D. Ren, *Theory of Orlicz Spaces*, Pure and Appl. Math., Marcel Dekker Inc. New York-Basel-Hong Kong, 1991.
[45] C. Bardaro, G. Vinti, *Some Inclusion Theorems for Orlicz and Musielak-Orlicz Type Spaces*, Annali di Matematica Pura e Applicata, **168** (1995), 189–203.
[46] M. M. Rao, Z. D. Ren, *Applications of Orlicz Spaces*, Monographs and Textbooks in Pure and applied Mathematics, vol. 250, Marcel Dekker Inc., New York, 2002.
[47] G. Vinti, L. Zampogni, *Approximation by means of nonlinear Kantorovich sampling type operators in Orlicz spaces*, Journal of Approximation Theory, **161** (2009), 511–528.
[48] C. Donnini, G. Vinti, *Approximation by Means of Kantorovich Generalized Sampling Operators in Musielak-Orlicz spaces*, PanAmerican Mathematical Journal, **18** (2) (2008), 1–18.
[49] G. Vinti, L. Zampogni, *A Unifying Approach to Convergence of Linear Sampling Type Operators in Orlicz Spaces*, Advances in Differential Equations, **16** (5-6) (2011), 573–600.
[50] G. Vinti, L. Zampogni, *A unified approach for the convergence of linear Kantorovich-type operators*, in print in:

Nonlinear Advanced Studies (2014).
[51] F. Ventriglia, G. Vinti, *A unified approach for the convergence of nonlinear Kantorovich type operators*, Communications on Applied Nonlinear Analysis, 21 (2) (2014), 45–74.
[52] C. Bardaro, I. Mantellini, *On convergence properties for a class of Kantorovich discrete operators*, Numerical Functional Analysis and Optimization, **33** (4) (2012), 374–396.
[53] D. Costarelli, G. Vinti, *Order of approximation for sampling Kantorovich operators*, to appear in: Journal of Integral Equations and Applications (2014).
[54] D. Costarelli, G. Vinti, *Order of approximation for nonlinear sampling Kantorovich operators in Orlicz spaces*, Commentationes Mathematicae, Special number dedicated to Prof. Julian Musielak, 53 (2) (2013), 271–292.
[55] F. Cluni, D. Costarelli, A.M. Minotti, G. Vinti, *Applications of sampling Kantorovich operators to thermographic images for seismic engineering*, in print in: Journal of Computational Analysis and Applications (2014).
[56] D. Costarelli, G. Vinti, *Approximation by Nonlinear Multivariate Sampling Kantorovich Type Operators and Applications to Image Processing*, Numerical Functional Analysis and Optimization, **34** (8) (2013), 819–844.
[57] P.L. Butzer, R.J. Nessel, *Fourier Analysis and Approximation, I*, Academic Press, New York-London, 1971.
[58] P.L. Butzer, W. Engels, S. Ries, R.L. Stens, *The Shannon sampling series and the reconstruction of signals in terms of linear, quadratic and cubic splines*, SIAM Journal on Applied Mathematics, **46** (1986), 299–323.
[59] D. Costarelli, R. Spigler, *Approximation by series of sigmoidal functions with applications to neural networks*, to appear in: Annali di Matematica Pura e Applicata, (2013) DOI: 10.1007/s10231-013-0378-y.
[60] D. Costarelli, R. Spigler, *Approximation results for neural network operators activated by sigmoidal functions*, Neural Networks, 44 (2013) 101–106.
[61] D. Costarelli, R. Spigler, *Multivariate neural network operators with sigmoidal activation functions*, Neural Networks, 48 (2013), 72–77.
[62] D. Costarelli, R. Spigler, *Convergence of a family of neural network operators of the Kantorovich type*, Journal of Approximation Theory, 185 (2014) 80–90.
[63] D. Costarelli, *Interpolation by neural network operators activated by ramp functions*, Journal of Mathematical Analysis and Application, 419 (1) (2014) 574–582.
[64] N. Cavalagli, F. Cluni, V. Gusella, *Evaluation of a Statistically Equivalent Periodic Unit Cell for a quasi-periodic masonry*, International Journal of Solids and Structures, **50** (2013), 4226–4240.
[65] R. Gonzales, R. Woods, *Digital Image Processing*, Prentice-Hall NJ - USA, 2002.
[66] R. Hill, *Elastic properties of reinforced solids: some theoretical principles*, Journal of the Mechanics and Physics of Solids, **11** (1963), 357–372.
[67] F. Cluni, V. Gusella, *Homogenization of non-periodic masonry structures*, International Journal of Solids and Structures, **41** (2004), 1911–1923.
[68] J. Aboudi, *Mechanics of Composite Materials: A Unified Micromechanical Approach*, Elsevier, Amsterdam, 1991
[69] *2008 Italian Building Code — Norme Tecniche per le Costruzioni* (in Italian), published on the Official Gazette of the Italian Republic nr. 29 of 4/2/2008, 2008.
[70] M. Ottaviani, *Proprietà geotecniche di tufi vulcanici italiani* (in Italian), Rivista Italiana di Geotecnica, **3**/88 (1988), 173–178.
[71] C.J. Sachpazis, *Correlating Schmidt Hardness With Compressive Strength and Young's Modulus of Carbonate Rocks*, Bulletin of the International Association of Engineering Geology, **42** (1990), 75–83.